X-ray Diffuse Scattering from Interfaces in Semiconductor Multilayers

Sergey Stepanov

Illinois Institute of Technology, BioCAT at the Advanced Photon Source
9700 S. Cass Ave., Bldg.435B, Sector 18, Argonne, IL 60439

Abstract. Several recent studies on x-ray scattering from interface roughness in epitaxial semiconductor multilayers are reviewed. The discussion is focused on the new effects specific to the roughness in crystals that have been found in these studies. These include the anisotropy in scattering due to the dependence of roughness on crystallographic directions and the asymmetry due skew roughness transfer in molecular beam epitaxy and the staircase atomic structure of vicinal interfaces. In addition, roughness effects on Bragg diffraction from crystals and the related opportunities to measure crystal lattice strains inside roughness are discussed.

1. INTRODUCTION

Nowadays non-specular X-ray scattering (XRS) is commonly recognized as one of the most convenient techniques for the studies of interface roughness. On the other hand, interface quality is known as the crucial parameter in microelectronics based on semiconductor multilayers. Therefore, a wide range of XRS applications to microelectronics is foreseen with possible valuable technological output.

This report reviews several recent studies [1,2] by the author on x-ray scattering from MBE-grown semiconductor multilayers. The review is complemented with some recent yet unpublished results.

In Section 2 we analyze the effects specific to XRS from semiconductor multilayers that require modifications to the XRS theory that was originally developed for amorphous structures. In particular, the anisotropy and asymmetry in XRS are discussed in relation to the scattering from atomic steps and step bunches and the skew interface-interface roughness transfer in MBE-grown multilayers. The discussion is illustrated with XRS data and respective theoretical simulations for MBE-grown AlAs/GaAs multilayers.

In Section 3 we discuss the scattering from roughness under the grazing-incidence diffraction from crystalline multilayers. In crystals, one can study XRS not only at specular reflection, but also at Bragg diffraction from atomic planes. This combination provides additional opportunities for roughness characterization. It will be shown how the measurements of XRS at grazing incidence diffraction can bring the data on crystal structure perfection inside roughness bumps.

Finally, Section 4 discusses XRS from interface roughness in symmetric and extremely asymmetric x-ray diffraction geometries. This is related to the opportunity of measuring crystal lattice strains inside roughness.

In Conclusions, the information is provided how to analyze the XRS data via the World Wide Web.

2. SPECIFICS OF X-RAY DIFFUSE SCATTERING FROM SEMICONDUCTOR MULTILAYERS

As known, originally the applications of XRS technique to the studies of roughness were based on the self-affine roughness model by Sinha *et al* [3]. According to this model the roughness causes non-specular x-ray scattering round the specular reflection rod (Fig.1).

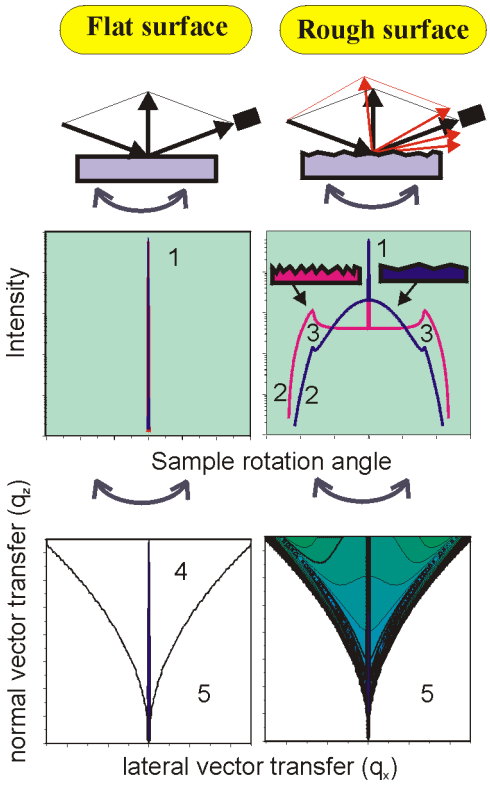

FIGURE 1. Illustration of rocking curves (upper) and intensity maps (lower) of x-ray scattering from rough surface. 1: specular peak, 2: diffuse scattering curves, 3: Yoneda peaks of diffuse scattering at critical angle for total reflection, 4 and 5: regions of reciprocal space accessible and inaccessible respectively in x-ray scattering experiment.

On Fig.1 one can see the basic features of XRS from self-affine roughness. First, the larger is the lateral size of roughness bumps (the so-called lateral correlation length of roughness), the smaller are the XRS deviations from the rod and vice versa (clearly, the infinitely wide fluctuations can be viewed as a flat surface and produce the specular rod only). Second, the XRS pattern is symmetric over the deviations of sample from the specular reflection position (given the directions of the incident and scattered waves are fixed).

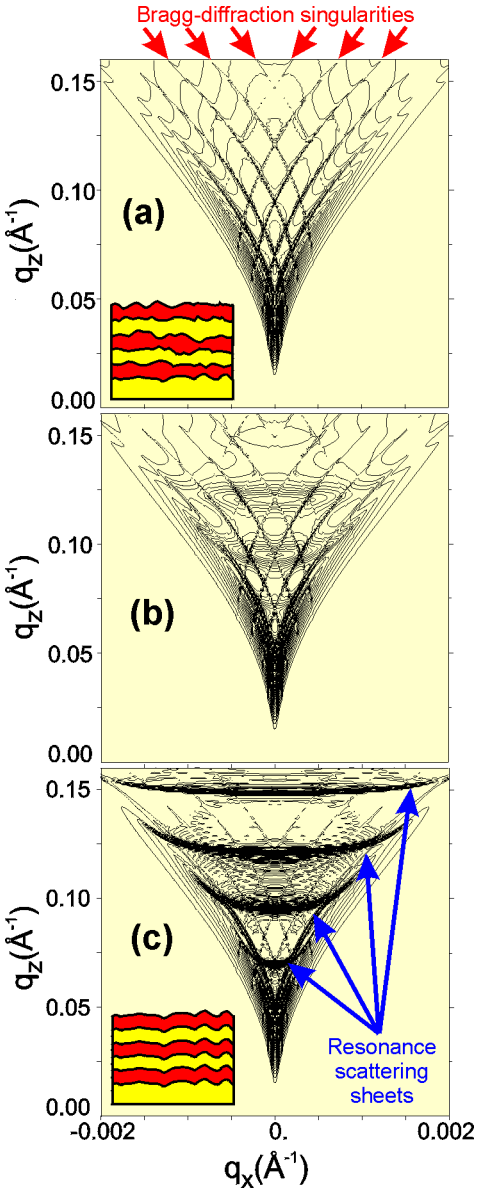

FIGURE 2. Formation of resonance sheets ("bananas") in the diffuse scattering with the increase of vertical correlation between roughness of different interfaces in periodic multilayers. The calculations are for a AlAs/GaAs superlattice with 20 periods. (a): no vertical correlation, (b): vertical correlation of 1 multilayer period (200Å), (c): complete

vertical correlation. The illustration is taken from [5].

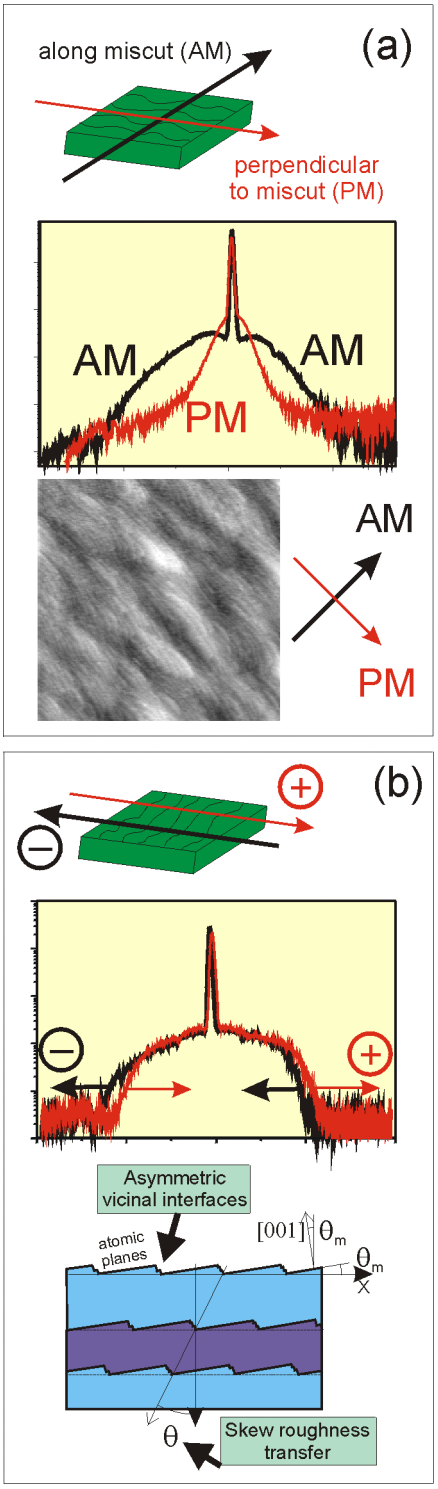

FIGURE 3. Effects of anisotropy (a) and asymmetry (b) in diffuse scattering from the roughness of epitaxially grown crystalline multilayers.

This follows from the reciprocity theorem and the fact that surface relief looks statistically identical for the incident and inverted scattered waves. Finally, usually the roughness of amorphous samples is isotropic (unless it is artificially produced) and therefore XRS pattern does not change at sample rotations round its surface normal.

The above features are also preserved for multilayers with multiple rough interfaces. In addition some new effects may arise when the roughness of different interfaces is correlated. These effects are most clearly displayed in periodic multilayers that are a frequent practical case of samples. On Fig.2 one can see the effect of vertical roughness correlation on XRS: the formation of horizontal bunches (or so-called Holy bananas [4]) of diffuse scattering with the increase in the vertical correlation between roughness of different interfaces.

Now, let us proceed to the topic of this report – to the roughness of heteroepitaxial semiconductor multilayers where the layers are monocrystals. We take the superlattices grown by molecular beam epitaxy (MBE) as an example. Such samples are normally grown on single crystal substrates with a small miscut of the surface from a basic crystallographic plane, e.g. (100). The miscut determines the direction of atomic steps flow at the surface thus providing a more stable and reproducible growth conditions. On the other hand, the interface relief of such multilayers consists of terraces elongated in the direction perpendicular to the miscut and separated by the steps and step bunches in the miscut direction (see the sketch and the AFM image of the surface on Fig.3a).

Due to this anisotropy of interfaces, the XRS data taken in the directions along and perpendicular to the miscut (AM and PM respectively) look different (Fig.3a) and

one can measure with XRS the size of terraces in the two directions.

Table I: Growth conditions and structure of AlAs/GaAs superlattices 1 to 4				
GaAs (001) substrate:	**Sample 1**	**Sample 2**	**Sample 3**	**Sample 4**
- surface miscut angle [°], ± 0.03	**0.38**	**0.40**	**0.43**	**0.38**
- deviation of miscut from [110] [°], ±5	**8**	**5**	**0**	**6**
- GaAs buffer layer thickness [Å]	**1000**	**1000**	**2000**	**5000+206**
Superlattice preparation:	**Sample 1**	**Sample 2**	**Sample 3**	**Sample 4**
-Growth temperature [° C]	**610**	**610**	**580**	**610**
- As_4 / Ga beam equiv. Pressure ratio	**12**	**15**	**17**	**7**
- Growth rate [µm / h]	**0.5**	**0.5**	**0.5**	**0.5**
- Growth mode of GaAs layers	**step flow**	**step flow/2D nucl.**	**2D nucleation**	**step flow**
- Growth interruption after GaAs [s]		**120**		**120**
Superlattice parameters:	**Sample 1**	**Sample 2**	**Sample 3**	**Sample 4**
- Number of periods of AlAs/GaAs	**20**	**20**	**20**	**20**
- AlAs layer thickness [Å], ± 0.5	**156.0**	**153.3**	**160.0**	**154.2**
- GaAs layer thickness [Å], ± 0.5	**71.0**	**71.0**	**68.0**	**70.8**
- surface oxide thickness [Å], ± 1	**18**	**15**	**15**	**12**
- total rms roughness [Å], ±0.5	**4.0**	**4.0**	**3.5**	**3.0**
- surface rms roughness [Å], ±0.2	**4.2**	**4.7**	**3.3**	**2.3**

Table II: X-ray scattering results for AlAs/GaAs superlattices 1 to 4				
Along miscut:	**Sample 1**	**Sample 2**	**Sample 3**	**Sample 4**
- lateral correlation length 1(2) [Å], ± 250	**2000(1000)**	**2500(1000)**	**4000**	**5000**
- roughness exponent (jaggedness), ± 0.1	**0.8**	**0.75**	**0.9**	**0.9**
- vertical correlation length 1(2) [Å], ± 250	**3000(3000)**	**1500(1000)**	**2000**	**1000**
- skew inheritance angle [°], ± 5	**-15**	**-45**	**45**	**45**
- relative correlated roughness [%]	**100**	**100**	**100**	**40**
Perpendicular to miscut:	**Sample 1**	**Sample 2**	**Sample 3**	**Sample 4**
- lateral correlation length 1 [Å], ± 250	**4000**	**7000**	**3500**	**6000**
- roughness exponent (jaggedness), ± 0.1	**0.75**	**0.85**	**0.9**	**0.9**
- vertical correlation length 1 [Å], ± 250	**3000**	**1500**	**2000**	**1000**
- skew inheritance angle [°], ± 5	**8**	**75**	**10**	**50**
- relative correlated roughness [%]	**100**	**100**	**100**	**40**

Another new feature of roughness in crystalline multilayers is demonstrated on Fig.3b. The curves of XRS measured along the miscut direction may be asymmetric and the asymmetry inverts at turning the sample by 180° around its surface normal. This effect first discussed in [7-9] can have the two possible explanations, as illustrated at Fig.3b: either it is due to the asymmetry of interfaces with respect to the "+" and "–" directions of incident x-rays or to a skew roughness inheritance by successive interfaces.

We have analyzed the relevance of the two models for a series of four MBE grown AlAs/GaAs multilayers [2]. A more detailed information about the samples is given in Table-I and the results of our study are shown on Fig.4 to 7 and summarized in Table II.

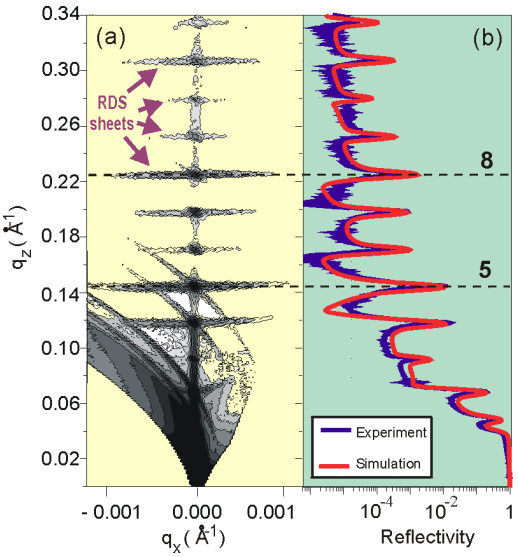

FIGURE 4. Reciprocal space map of diffuse scattering measured from a AlAs/GaAs superlattice (a) and the respective specular reflectivity curve (the section of the map along q_z at q_x=0). Numbers 5 and 8 mark the resonance sheets analyzed in the experiment and shown on Fig.5 to 7. Borrowed from [2].

Fig.4 presents a general view of XRS map in the reciprocal space for one of the samples. It is well seen that the XRS is strictly bunched into horizontal strips (the resonance diffraction sheets, RDS), which indicates a high degree of interface-interface roughness correlations in the sample. This result is reproduced for all the four samples grown with different growth conditions. The numbers 5 and 8 on the figure mark the two RDS that were studied with high resolution and plotted on Figs.5 and 7. These high-resolution plots show that the XRS measured along the miscut direction is asymmetric and the asymmetry inverts when switching from "+" to "–" direction of incident x-rays. If one drew the sections of these maps along q_x, he would get the asymmetric curves shown on Fig.3b. However, the maps provide a better understanding for the effect: they show that the asymmetry arises due to the deviation of RDS from the horizontal plane.

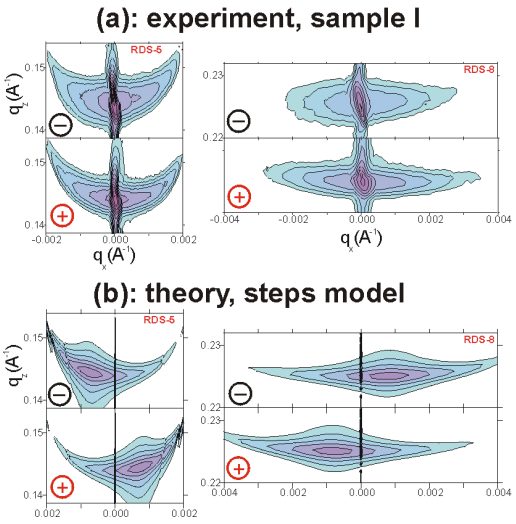

FIGURE 5. Comparison of measurements for sample-I with the calculations assuming that the asymmetry is due to regular atomic steps on vicinal interfaces (the generalized Pukite model).

Fig.5b shows the attempt to fit the data with the model assuming that XRS asymmetry is due to the staircase structure of interfaces. The calculations use the correlation function by Pukite, Lent and Cohen [9] generalized in [2] for possible step bunches. One can see that indeed the calculated RDS look inclined as needed, but they also shift horizontally along q_x and the latter effect is not observed in the experiment. The calculation of the whole XRS map with this model (Fig.6) demonstrates that XRS from atomic staircase is concentrated along the skew line which is perpendicular to the facets on interfaces (i.e. to the basic crystallographic plane) while the specular rod is perpendicular to the mean surface. The angle between these two directions (the miscut angle) provides the q_x-shift of calculated RDS on Fig.5. This effect has also been discussed in Ref.[8].

Thus, we found that the staircase structure of interfaces is not responsible for the asymmetry of XRS from MBE-grown AlAs/GaAs multilayers. This effect, however, can be relevant for other types of semiconductor multilayers where a larger lattice constant mismatch between the

layers is resulted in a higher step bunches [10].

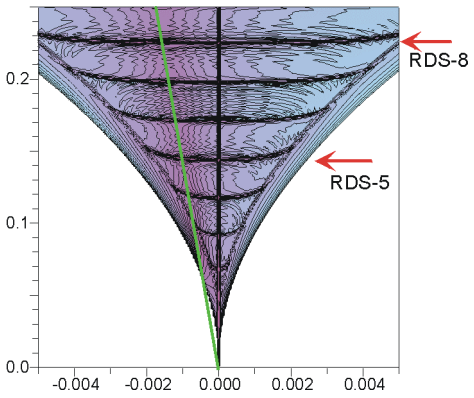

FIGURE 6. General view of diffuse scattering map calculated with the Pukite model. The black vertical line marks the specular rod and it is perpendicular to the surface. The skew line is the normal to the crystallographic plane forming the facets between the steps at the interfaces.

Fig.7 demonstrates that the experimental data can be well explained with the second model that assumes a skew roughness transfer between interfaces. The calculations use the self-affine roughness model by Sinha et al [3] corrected for the skew interface-interface roughness correlation:

$$K_{nn'}(x) \rightarrow K_{nn'}\left(x - \tan\theta\left[z_n - z_{n'}\right]\right). \quad (1)$$

Here $K(x)$ is the correlation function of interface roughness [3], x is coordinate in the interface plane, z_n–$z_{n'}$ is the distance between interfaces n and n', and θ is the angle of skew roughness transfer (see Fig.3).

The most probable physical explanation for the skew roughness transfer could be that the relief of the deeper interfaces is transferred to the successive ones by flowing steps. Then, the skew transfer could always be expected towards the step flow direction. However, in our experiment this was the case for samples III and IV only with a better substrate preparation and a lower rms roughness. Generally the value and the sign of angle θ depended on the growth conditions (Table II) and for samples I and II this angle was negative. We assume that it occurred due to a preferred inheritance of high roughness in samples I and II along some crystallographic direction, but a further study is required to verify this assumption. Finally, the skew roughness transfer was also found in the PM direction (see Fig.3a). The large values measured in this case (Table II) indicate the deviation of the direction of skew inheritance from the miscut direction.

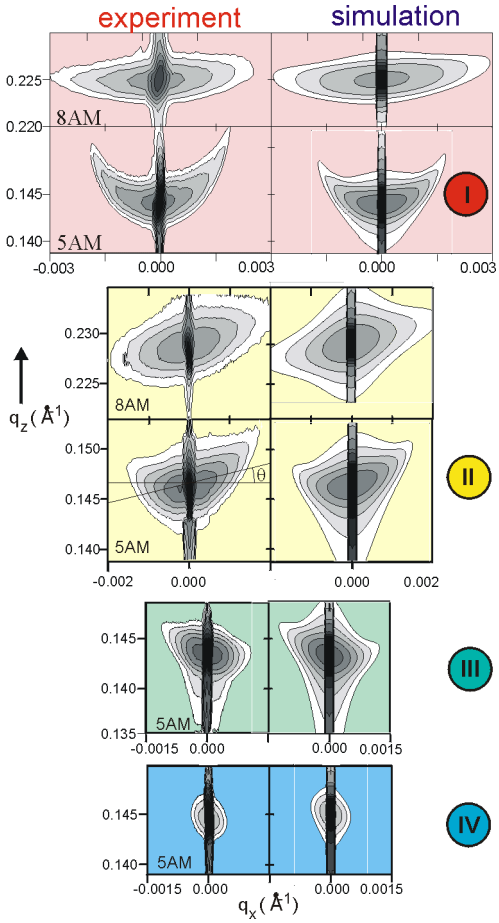

FIGURE 7. Experimental proof for skew roughness correlation in AlAs/GaAs superlattices [2]. The numbers I, II, III and IV mark the data for samples 1 to 4 respectively.

Along with the above discussed effects the XRS study revealed a number of dependencies of the lateral size and vertical correlation length of roughness on the growth mode of GaAs layers (step flow

versus 3D nucleation), the presence of growth interruptions and on some other growth parameters. For the details see Table II and Ref.[2]. Noticeably, the XRS study has been proven to be a powerful tool for the studies of semiconductor multilayers.

3. EFFECT OF ROUGHNESS ON GRAZING INCIDENCE X-RAY DIFFRACTION

Lattice strains in crystalline multilayers are commonly examined with x-ray Bragg diffraction. In particular the grazing incidence diffraction (GID) is used for studies of thin surface layers. The specific sensitivity of GID to lattice strains in thin surface layers is provided by the combination of Bragg condition with the specular reflection effect for grazing x-rays (Fig.8b).

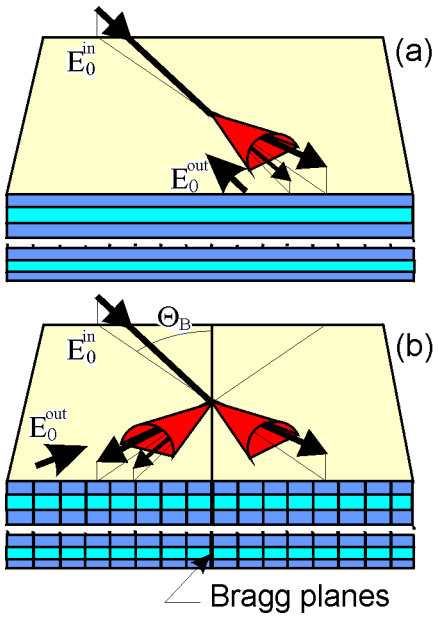

FIGURE 8. Schematic presentation of diffuse scattering in the specular reflection (a) and grazing incidence diffraction (b) experiments. The waves E^{out} are the virtual waves inverted with respect to the scattered ones. These waves are used for the calculation of diffuse scattering in the distorted wave Born approximation [1].

Since the grazing angles of x-rays to the surface in GID and in x-ray total external reflection (TER) experiments are the same, one can expect the same magnitude of XRS in both cases.

To calculate the XRS from roughness in GID we have used the distorted wave Born approximation analogous to that used in TER. The amplitude f of x-ray scattering from an interface fluctuation is calculated as [1]

$$f(\mathbf{r}) = \int \Psi^{out} \delta\chi(\mathbf{r}) \Psi^{in} \ , \qquad (2)$$

where Ψ^{in} and Ψ^{out} are x-ray wave fields produced in multilayer at the diffraction of the incident and inverted scattered waves respectively. The intensity of XRS from statistical roughness is a statistical average of contributions from all the fluctuations:

$$I \sim \langle f(\mathbf{r}_1) f(\mathbf{r}_2) \rangle \ . \qquad (3)$$

The substitution of (2) into (3) provides the expression for I via the correlation function of roughness:

$$K \sim \langle \delta\chi(\mathbf{r}_1) \delta\chi(\mathbf{r}_2) \rangle \qquad (4)$$

Eqs.(2) to (4) are general for TER and GID with the two exceptions:

1) In the case of TER Ψ^{in} and Ψ^{out} are the solutions to the specular reflection problem given by the Parratt recursive equations, while for GID the dynamical diffraction solution [2,11] must be used;

2) In the case of TER $\delta\chi(\mathbf{r}) \equiv \delta\chi_0(\mathbf{r})$ is determined by the difference in the dielectric susceptibility (the mean electron density) of two materials at interfaces, while for GID it also depends on the difference in the Bragg scattering amplitudes:

$$\delta\chi(\mathbf{r}) = \delta\chi_0 + \delta\chi_h e^{i\mathbf{hr}} + \delta\chi_{-h} e^{-i\mathbf{hr}} \qquad (5)$$

To verify the theory, we have carried out a GID experiment with a strained AlAs/GaAs superlattice [1]. The sample parameters were close to that listed in Tables I and II and the GID data were taken at the optical beamline of ESRF.

Fig. 9a shows the double-crystal rocking curve of GID superimposed on the dynamical diffraction calculation for multilayer with flat interfaces. The tails of

experimental curve run much higher than expected by the theory. Since the dynamical theory of GID is well proven, this discrepancy can be attributed to XRS that was integrated with the diffracted signal in the double-crystal measurements. The effect of diffuse scattering is especially clear at the left tail of rocking curve where the diffracted intensity must be zero due to the total *internal* reflection effect for diffracted wave. Then, all the intensity measured there must be due to diffuse scattering.

Fig.9b displays the calculated map of diffuse scattering from roughness in GID for this sample. The parameters of roughness used in the calculations were determined from the usual XRS measurements. The calculations employ the self-affine roughness model by Sinha *et al* and the assumption of complete vertical correlation of roughness in multilayer. Due to the latter assumption the calculated XRS forms the horizontal strips of resonance scattering at the exit angles corresponding to different order Bragg reflections from periodic multilayer. The vertical strip at $\theta-\theta_B=0$ is the minimum of XRS at the total *internal* reflection threshold (the anti-Yoneda effect, see [1]).

Fig.9c presents the high-resolution spectra of GID measured with a position sensitive detector. These curves correspond to the vertical sections of map at Fig.9b. The respective theoretical curves are shown by the dotted lines and the arrows mark the diffraction peaks. The agreement with the theory is quite satisfactory.

To our opinion, a possible application of XRS in GID is to determine the atomic ordering in roughness, as illustrated on Fig.10. X-ray scattering in usual TER experiment (Fig.10a) is not sensitive to the crystal structure of multilayers, while the scattering in GID depends on the degree of crystal perfection at interfaces through the $\delta\chi_h$ terms in (5). If atomic lattice is not distorted at interfaces (Fig.10b), then the parameters of roughness given by the TER experiment should fit the GID data as well. If, however, there is a lattice disorder in the roughness bumps, then χ_h is reduced by some static Debye-Waller factor and the XRS intensity measured in GID becomes lower than one would expect from the TER measurements. This a particular case of a more general result that the three terms in (5) may result in several different correlation functions contributing to Eq.(4) and consequently to XRS.

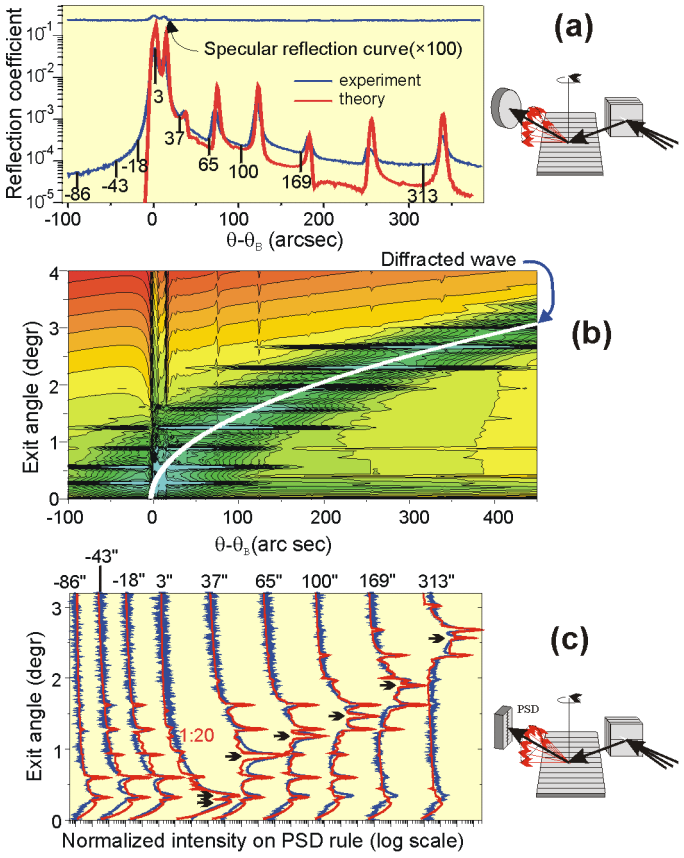

FIGURE 9. Measurements of diffuse scattering from interface roughness in grazing incidence diffraction [1]. The data are for MBE-grown AlAs/GaAs superlattice. (a): double crystal rocking curve, (b): calculated map of diffuse scattering, (c): the distributions of diffuse scattering over the exit angle measured with PSD at different points of the rocking curve (a).

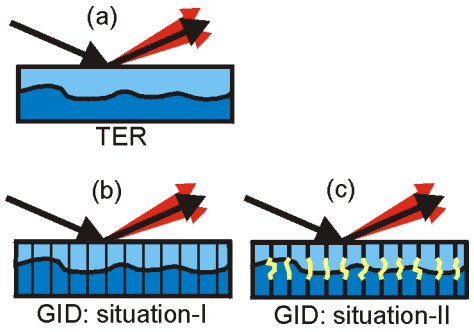

FIGURE 10. The difference between diffuse scattering in GID and specular reflection experiments: in the latter case the scattering is mainly from the Bragg planes inside the roughness bumps. This allows deciding in GID between the situations I and II respectively.

4. EFFECT OF LATTICE STRAINS IN ROUGHNESS ON ASYMMETRIC X-RAY DIFFRACTION

The effect of XRS from roughness may be expected not only for GID but for other diffraction geometries too. At least, one can anticipate a comparable intensity of XRS for extremely asymmetric x-ray diffraction where either the incident or diffracted wave are grazing in the range of specular reflection. However, here one must take into account the scattering from vertical strains.

Let us consider a general case of interface between two materials 1 and 2 with the dielectric susceptibilities χ_1 and χ_2 and the reciprocal lattice vectors $\mathbf{h}_1$ and $\mathbf{h}_2$ respectively. When a fluctuation at the interface takes place and material 2 replaces 1, this perturbation becomes a source of x-ray diffuse scattering at both x-ray specular reflection and Bragg diffraction. The amplitude of XRS in the Bragg diffraction is proportional to

$$\delta\chi(\mathbf{r}) = (\chi_{02} - \chi_{01}) + \left(\chi_{h2} e^{i\mathbf{h}_2(\mathbf{r})\mathbf{r}} - \chi_{h1} e^{i\mathbf{h}_1\mathbf{r}}\right) + \left(\chi_{-h2} e^{-i\mathbf{h}_2(\mathbf{r})\mathbf{r}} - \chi_{-h1} e^{-i\mathbf{h}_1\mathbf{r}}\right), \quad (6)$$

where $\mathbf{h}_2$ is written as a function of $\mathbf{r}$ because of possible strains in roughness.

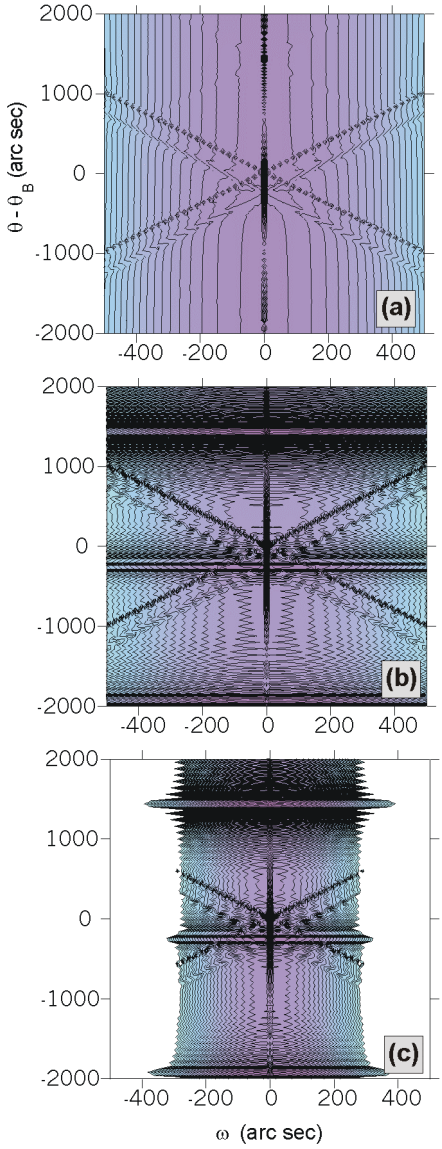

FIGURE 11. Calculated maps of diffuse scattering from interface roughness for 400 symmetric Bragg diffraction. The data are for AlAs/GaAs superlattice with 230Å period and 4Å rms roughness. (a): the lateral correlation of L=500Å and no vertical correlation; (b): same with complete vertical correlation; (c): L=1000Å and complete vertical correlation.

In the case of GID considered in Section 3, the $\mathbf{h}$ vector is parallel to the surface. Therefore, if there is no strain relaxation ($\mathbf{h}_2 = \mathbf{h}_1$; the multilayer does not contain misfit dislocations), only irregular strains are present and one can take

$$\left\langle \chi_{h2} e^{\pm i\mathbf{h}_2(\mathbf{r})\mathbf{r}} \right\rangle = \chi_{h2} e^{-W} e^{\pm i\mathbf{h}_1\mathbf{r}} \quad . (7)$$

Here exp(–*W*) is the static Debye-Waller factor reducing χ_h as discussed above. In this case we arrive at Eq.(5).

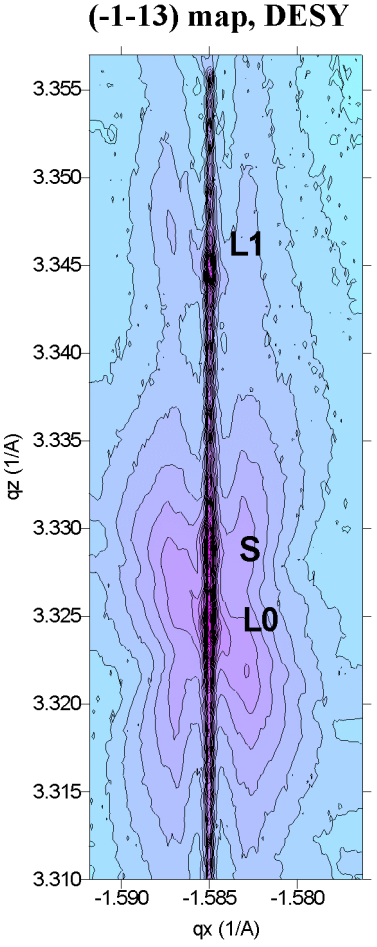

FIGURE 12. Experimental map of diffuse scattering from interface roughness of InGaP/GaAs measured around (-1-13) asymmetric Bragg reflection (presented by E.A. Kondrashkina). The letters S, L0, and L1 denote the substrate and the 0th and 1st order superlattice peaks respectively. The "butterfly" shape of diffuse resembles the structure predicted on Fig.11(b).

In asymmetric Bragg diffraction vector **h** has a vertical component which accommodates the difference in lattice parameters for materials 1 and 2. Then, for example, with the assumption $\delta h\, L << 1$ (L is the lateral scale of roughness) we obtain:

$$\delta\chi(\mathbf{r}) = \delta\chi_0 + \delta\chi_h e^{i\mathbf{h}_1\mathbf{r}} + \delta\chi_{-h} e^{-i\mathbf{h}_1\mathbf{r}} + (\delta\mathbf{h}(\mathbf{r})\cdot\mathbf{r})\left(\chi_{h2} e^{i\mathbf{h}_1\mathbf{r}} + \chi_{-h2} e^{-i\mathbf{h}_1\mathbf{r}}\right) . \quad (8)$$

For diffraction with large incidence and exit angles of x-rays to the surface (e.g. for the symmetric Bragg case) the $\delta\chi_0$ terms are known to have a small effect on x-ray scattering. Then, the strain effects given by the last term in Eq.(8) may become important.

Fig.11 presents the calculated effect of roughness on symmetric Bragg diffraction. The calculations exhibit the same basic peculiarities of XRS pattern (the horizontal resonance diffraction sheets for vertically correlated roughness, the concentration of scattering round the specular rod for large lateral correlation length of roughness and the presence of skew Bragg strips) as that at TER (compare Fig.2). As a matter of qualitative comparison Fig.12 shows the map of XRS from an InGaP/GaAs superlattice. The butterfly-like pattern on the experiment is obviously due to the Bragg strips like that on the calculated map, but being spread by strains.

Fig.11 is calculated yet without taking into account any strains. The models for strains in roughness (i.e. for $\delta\mathbf{h}(\mathbf{r})$) are still under development. See also Ref.[12] where the XRS is calculated as a DWBA correction to the kinematical Bragg diffraction theory.

5. CONCLUSIONS

We have reviewed some recent studies on x-ray scattering from interface roughness in semiconductor multilayers. It has been shown that the XRS is capable of delivering valuable and sometimes unique information about the structure of semiconductor interfaces. Due to possible applications in semiconductor research and technology, the XRS technique has received a lot of scientific efforts and in the past few years it has been developing very fast. While some basic effects like the XRS asymmetry and anisotropy have been

explained, the studies on others and especially on the contribution of lattice strains to XRS in the Bragg diffraction are still in progress.

In view of this dynamic development it is important to keep the experimental groups up to date with modern advances in the theory. Therefore we have developed a Web site where everyone can simulate his data using the most recent models for x-ray reflection, diffraction and scattering from semiconductor multilayers. The Web interfaces to new theoretical models appear at the server even before they get published. This allows to verify and improve the theory and the computation algorithms with the help of users feedback. The x-ray server address is http://sergey.bio.aps.anl.gov. Up to now the WWW interfaces to the following four programs have been implemented:

- X-ray Bragg diffraction from strained crystalline multilayers in various geometries including GID and coplanar and non-coplanar asymmetric x-ray diffraction.
- X-ray specular reflection from multilayers with interface roughness and transition layers
- X-ray diffuse scattering from interface roughness in amorphous and crystalline multilayers with 10 different models of lateral and vertical roughness correlations including those discussed in this report.
- A database of x-ray scattering and absorption factors needed for the analysis of diffraction and reflection data.

Fig.13 demonstrates an example of WWW input data form for the diffraction program. The other interfaces are similar.

During the two years of server operation these four programs have been called for more than 6000 times and found their permanent users. This statistics proves the efficiency of the idea. However, more users are always welcome to enter this Internet collaboration.

ACKNOWLEDGMENTS

This study was carried out in collaboration with many colleagues from several countries: E.Kondrashkina, R.Köhler, R.Opitz, U. Pfeiffer and M.Schmidbauer *(Humboldt University, Berlin)*, R.Hey, M.Wassermeier and V.Kaganer *(PDI, Berlin)*, G.Materlik, D.Novikov and H.Rhan *(DESY, Hamburg)*, T.Baumbach and A.Souvorov *(ESRF, Grenoble)*, S.Durbin *(Purdue University, West Lafayette)*, T.Jach (*NIST, Gaithersburg*), U.Pietsch (*Potsdam University*), and A.Ulyanenkov (*Minsk University*). Their valuable contribution is greatly appreciated. I would also like to acknowledge extremely stimulating discussions with J.Hartwig and U.Lienert *(ESRF, Grenoble)*, A.Macrander and S.Sinha *(ANL, Argonne)*, A.Chernov *(Institute of Crystallography, Moscow)*, V.Holy *(Masaryk University, Brno)*, V.Kohn *(Kurchatov Institute, Moscow)*, H.Raidt *(Humboldt University, Berlin)*.

REFERENCES

[1] S.A. Stepanov, E.A. Kondrashkina, M. Schmidbauer, R. Köhler, J.-U. Pfeiffer, T. Jach, and A.Yu. Souvorov, Phys. Rev. B **54**, 8150 (1996).

[2] E.A. Kondrashkina, S.A. Stepanov, R. Opitz, M. Schmidbauer, R. Köhler, R. Hey, M. Wassermeier, and D.V. Novikov, Phys. Rev. B **56**, 10469 (1997).

[3] S.K. Sinha, E.B. Sirota, S. Garoff, and H.B. Stanley, Phys. Rev. B **38**, 2297 (1988).

[4] V. Holy and T. Baumbach, Phys. Rev. B **94**, 10669 (1994).

[5] V.M. Kaganer, S.A. Stepanov, and R. Köhler, Phys. Rev. B **52**, 16369 (1995).

[6] R.L. Headrick and J.M. Baribeau, Phys. Rev. B **48**, 9174 (1993)

[7] Y.H. Phang, C. Teichert, M.G. Lagally, L.J. Peticolos, J.C. Bean, and E. Kasper, Phys. Rev. B **50**, 14435 (1994)

[8] S.K. Sinha, M.K. Sanyal, S.K. Satija, C.F. Majkrzak, D.A. Neumann, H. Homma, S. Szpala, A. Gibaud, and H. Morkoc, Physica B **198**, 72 (1994)

[9] P.R. Pukite, C.S. Lent, and P.I. Cohen, Surface Science, 161, 39 (1985)
[10] V. Holy, C. Giannini, L. Tapfer, T. Marschner, and W. Stolz, Phys. Rev. B **55**, 9960 (1997).
[11] S.A. Stepanov, E.A. Kondrashkina, R. Köhler, D.V. Novikov, G. Materlik, and S.M. Durbin, Phys. Rev. B **57**, 4829 (1998).
[12] V. Holy, A.A. Darhuber, J. Stangl, S. Zerlauth, F. Schaeffler, G. Bauer N. Darowski, D. Luebbert, U. Pietsch and I. Vavra, Phys. Rev. B **58**, 7934 (1998).

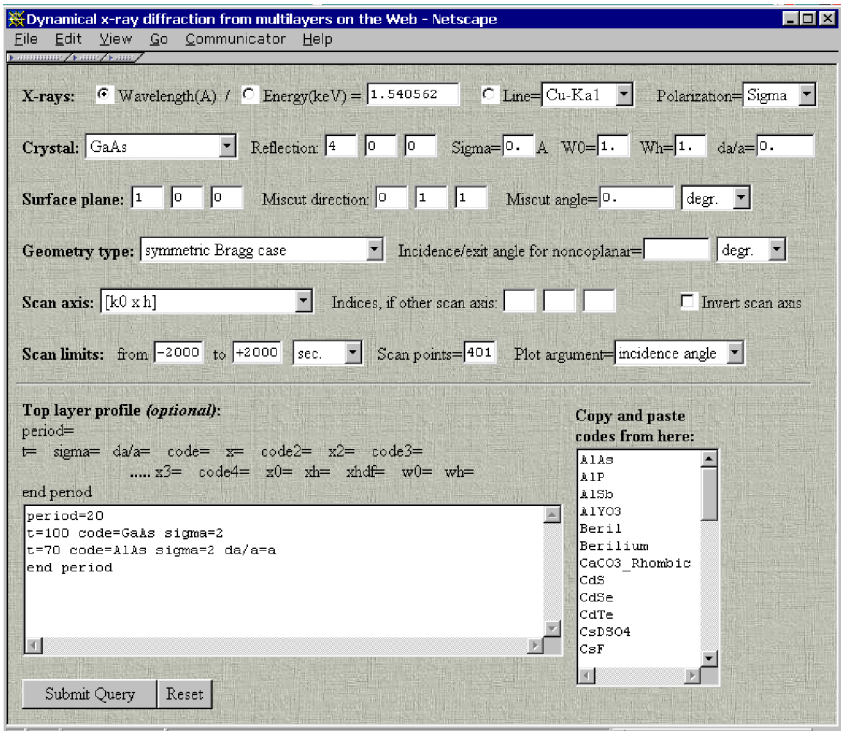

FIGURE 13. An example of Web form for the online calculations of x-ray Bragg diffraction at http://sergey.bio.aps.anl.gov. Similar forms are also provided for x-ray specular reflection from multilayers and diffuse scattering from interface roughness.